

A Fast Multistream Scattering-Based Jacobian for Microwave Radiance Assimilation

Alexander G. Voronovich, Albin J. Gasiewski, *Fellow, IEEE*, and Bob L. Weber

Abstract—The full utilization of satellite-based passive microwave imagery for weather forecasting rests on the ability to assimilate radiances into numerical weather prediction (NWP) models for highly scattering and absorbing hydrometeor states. State vector updates need to be performed rapidly enough to maintain pace with the sensor data stream and require, in particular, rapid calculation of the tangent linear relationship (Jacobian) between the observed antenna temperatures and the NWP prognostic hydrometeor parameters. To facilitate the use of both spaceborne and airborne passive microwave data in numerical forecasting, we present a new rapid multiple-stream discrete-ordinate algorithm for calculating the Jacobian under arbitrary scattering and absorbing conditions. The algorithm is based on the layer-adding method for a plane-parallel atmosphere for which the number of operations required to compute the solution is proportional to the number of layers. A nontrivial aspect of the problem is the stable calculation of the reflectance and transmittance operators in highly scattering layers for which a diagonalization technique and analytical factorization of specific matrices are used to ensure stability. Scaling calculations suggest that the new algorithm will be suitable for use in real-time all-weather microwave radiance assimilation.

Index Terms—Assimilation, Jacobian, microwave, radiance.

I. INTRODUCTION

SPACEBORNE passive microwave sensors provide a unique means of measuring atmospheric and surface variables due to their ability to observe through clouds over a predictable and wide range of probing depths (e.g., [1]). Useful passive microwave channels for measurement of atmospheric or surface variables are located at window, O_2 , and H_2O absorption bands from as low as 1.4 GHz [2] to over 1500 GHz [3]. Data from such sensors are regularly used, for example, to measure temperature and moisture profiles in regions opaque to infrared (IR) sounders [4] and to map rainfall rate. Although rainfall measurements are most accurate within convectively driven systems and over a water background [5], passive microwave data have also been proven valuable in measuring rainfall rate and other useful raincell parameters over land and snow backgrounds [6], [7]. Other important satellite microwave observables include ocean

surface wind speed and direction [8]–[10] and cloud water and ice path [11], [12].

Several low-earth orbiting passive microwave sensors are maintained for operational weather nowcasting and forecasting purposes, including the Advanced Microwave Sounding Unit A/B sensors on the National Oceanic and Atmospheric Administration (NOAA)–15, –16, and –17 spacecraft, and the Special Sensor Microwave/Imager (SSM/I) and the Special Sensor Microwave/Temperature Sounder 2 (SSM/T-2) on the U.S. Defense Meteorological Satellite Program (DMSP) spacecraft. Additional sensors planned for operational weather forecasting include the NOAA Polar-orbiting Operational Environmental Satellites (NPOES) Conical-Scanning Microwave Imager/Sounder (CMIS) and Advanced Technology Microwave Sounder (ATMS) sensors [13]. Passive microwave sensors designed for research purposes but potentially useful for operational weather forecasting include the National Aeronautics and Space Administration (NASA) Tropical Rainfall Measuring Mission (TRMM) Microwave Imager, the U.S. Navy WindSat [14] sensor, and the Advanced Microwave Scanning Radiometer E (AMSR-E) and AMSR sensors on the NASA Aqua and the National Space Development Agency of Japan (NASDA) Advanced Earth Observing Satellite (ADEOS) platforms [15]. The stream of data from polar orbiting passive microwave satellites, thus, provides frequent global coverage with particularly high density at the higher latitudes.

While data from passive microwave satellites have been proven valuable in retrievals, their use for directly updating operational numerical weather prediction (NWP) models via radiance assimilation has been limited to cases of either clear air or mostly thin, nonscattering clouds. There are several reasons for this limitation, including the inability of existing operational NWP models to simulate subgrid cloud and precipitation dynamics [16], [17] accurately enough to predict satellite microwave data, and challenges in updating either 3D-var or 4D-var NWP models [18], [19] while maintaining both thermodynamic consistency and numerical stability. As a result, the full potential of microwave data in locating regions of heat and momentum transfer (as determined by the presence of precipitation, either convective or stratiform) and in improving knowledge of the thermodynamic state and frontal boundaries within heavy clouds remains untapped. In clear air, there are no significant advantages of microwave signals relative to IR signals for improving the thermodynamic state, and future IR sounders (e.g., [20]) will further extend IR capabilities to even broken cloud fields. For continuous and/or heavy clouds and precipitation, however, the information within microwave data is essential.

To extend microwave radiance assimilation to meteorological regions where it would be of greatest value—e.g., pre- and post-

Manuscript received September 26, 2003; revised March 30, 2004. This work was supported in part by the National Oceanic and Atmospheric Administration (NOAA) Oceanic and Atmospheric Research (OAR) and in part by the NOAA–NASA Joint Center for Satellite Data Assimilation (JCSDA).

A. G. Voronovich and A. J. Gasiewski are with the Environmental Technology Laboratory, Division of Microwave Systems Development, National Oceanic and Atmospheric Administration, Boulder, CO 80305-3328 USA (e-mail: alexander.voronovich@noaa.gov).

B. L. Weber is with the Science and Technology Corporation, Environmental Technology Laboratory, National Oceanic and Atmospheric Administration Boulder, CO 80305-3328 USA.

Digital Object Identifier 10.1109/TGRS.2004.830637

frontal zones, occluded landfalling jets, hurricane rainbands, and other cloud-covered forecast-sensitive regions—it is necessary (among other things) to perform fast calculations of the incremental sensor response functions for all meteorological conditions. Maximum *a posteriori* estimation of the optimal change in an NWP model's background state vector \bar{x}_b using a satellite observation vector \bar{y} can be based on the minimization of a cost functional $J(\bar{x})$

$$J(\bar{x}) = (\bar{x} - \bar{x}_b)^T \bar{B}^{-1} (\bar{x} - \bar{x}_b) + (\bar{y} - \bar{h}(\bar{x}))^T \bar{R}^{-1} (\bar{y} - \bar{h}(\bar{x})) \quad (1)$$

where \bar{x} is the adjusted state vector, \bar{B} is the NWP model state error covariance matrix (generally a function of the state vector \bar{x}_b), \bar{R} is the satellite sensor and forward radiative transfer model error covariance matrix, $\bar{h}(\bar{x})$ is the mapping from the NWP state vector to sensor observable, and superscript T denotes transposition. For passive microwave sensors, $\bar{h}(\bar{x})$ represents both the forward radiative transfer and antenna pattern convolution processes, and is both an injective and nonlinear mapping. A Bayesian solution \bar{x}_a to the minimization problem can be shown to be

$$\bar{x}_a = \bar{x}_b + (\bar{B}^{-1} + \bar{H}^T \bar{R}^{-1} \bar{H})^{-1} \bar{H}^T \bar{R}^{-1} (\bar{y} - \bar{h}(\bar{x}_b)) \quad (2)$$

where $\bar{H} = \partial \bar{h}(\bar{x}) / \partial \bar{x}$ is the tangent linear approximation to the observation process \bar{h} or the *Jacobian* of the process.

Currently, the fraction of data from spaceborne passive microwave sensors that can be assimilated into NWP models remains limited in part due to an inability to rapidly and accurately compute the Jacobian over heavy clouds and precipitation and for all significant prognostic variables. This limitation necessarily leads to poor minimization of J over such regions. For example, 1D-var retrievals of humidity, ocean surface wind speed, and cloud liquid water path were successfully demonstrated in an NWP environment using SSM/I data [21], but limited to cloud densities below $0.4 \text{ kg} \cdot \text{m}^{-2}$. Beyond this density, the cost function J exceeded the number of observational degrees of freedom. A comprehensive forward transfer model and Jacobian incorporating both absorption and scattering are required to provide both an appropriate number of degrees of freedom in the modeled sensor field and the capability to minimize J . In addition to radiance assimilation, the Jacobian is valuable for nonlinear retrievals wherein the background atmospheric and surface states are determined from an NWP model, climatology, or other related means.

In general, the Jacobian can be described using the chain rule as a product of three components

$$\bar{H} = \bar{H}_I \bar{H}_R \bar{H}_G \quad (3)$$

where the three subscripts I , R , and G denote Jacobian components connecting (respectively): (I) variations in the instrument response to variations in the radiance field, (R) variations in the radiance field to variations in the fundamental electromagnetic parameters of the atmosphere or surface, and (G) variations in the fundamental electromagnetic parameters to variations in the NWP prognostic variables. These components are termed the *instrument*, *radiation*, and *geophysical* Jacobians, respectively. Thus, \bar{H}_R is the partial derivative matrix of the solution of the

differential radiative transfer equation (DRTE) with respect to temperature and all bulk absorption, scattering, phase matrix, and surface bistatic scattering parameters. Although all three components of \bar{H} are required to solve (1) and (2), we focus here on a new method for rapid and accurate calculation of the radiation Jacobian \bar{H}_R .

Current numerical techniques used to calculate \bar{H}_R for scattering media have been based on either approximations using only two streams of radiation [22] or other more exact but relatively slow techniques (e.g., numerical differences [23] or perturbation solutions [24]). It has been shown, however, that neglect of the angular dependence of the radiation field in the two-stream model leads to overestimation of the cloud-top albedo. This error is the result of underestimating the mean free path of photons reflected at the cell top and can cause underestimation of brightness temperatures by up to 20–30 K at opaque 118-GHz channels [25]. Use of multiple streams (e.g., [26]) solves this problem but at greater computational expense, particularly if direct matrix inversion is used. The problem can also be solved for specific cases using a two-stream model with δ -scaling [27], but the solution is not guaranteed to be general.

In this paper, we discuss a new discrete-ordinate multiple-stream method for solving the DRTE for a plane parallel atmosphere based on the layer-adding method [29]. The atmosphere is represented as a stack of horizontal layers with constant properties within each layer. The solution of the direct problem is represented in the form of explicit recurrence relations. As such, differentiation of the solution with respect to the fundamental electromagnetic parameters is straightforward. A nontrivial aspect is calculation of the Jacobian with a number of operations proportional to the number of layers N , and not to N^2 as would be in a divided difference approach. Another nontrivial aspect is the stable calculation of reflectance and transmittance operators for both highly scattering and nearly transparent individual layers (e.g., [28]). The solution requires the calculation of exponential matrix functions carried out in a diagonal representation of appropriate operators. The operators are represented as the product of pairs of symmetric positive-definite matrices; thus, the diagonalization involves only symmetric matrices for which standard numerical procedures exist. Notwithstanding, direct application of the appropriate analytic expressions for the reflectance and transmittance operators of individual layers requires inversion of a particular matrix, which becomes ill-conditioned for radiometrically thick layers. To accurately compute the inverse for all cases of opacity and albedo, we perform an analytic factorization of this matrix. Using the factored matrix, the numerical stability of the overall solution is maintained without restriction.

II. SYMMETRIZED NUMERICAL DRTE

The DRTE for the brightness temperature $T_B(\theta, z)$ in a planar stratified atmosphere and for a single polarization takes the following form [30]:

$$\begin{aligned} \cos \theta \frac{dT_B(\theta, z)}{dz} = & -\kappa_e(z) T_B(\theta, z) + \kappa_a(z) T_{\text{atm}}(z) \\ & + \kappa_s(z) \int_0^\pi p(\theta, \theta', z) T_B(\pi - \theta', z) \sin \theta' d\theta' \quad (4) \end{aligned}$$

where κ_a is the absorption coefficient, κ_s is the scattering coefficient, $\kappa_e = \kappa_a + \kappa_s$ is the extinction coefficient, and $T_{\text{atm}}(z)$ is the thermodynamic atmospheric temperature. These parameters, along with the normalized azimuthally averaged scattering phase function $p(\theta, \theta', z)$ are generally functions of height z . All angular dependencies can be considered to be functions of the variable $\mu = \cos \theta$ rather than the direction of propagation θ itself. Accordingly, we obtain

$$\mu \frac{dT_B(\mu, z)}{dz} = -\kappa_e(z)T_B(\mu, z) + \kappa_a(z)T_{\text{atm}}(z) + \kappa_s(z) \int_{-1}^1 p(\mu, \mu', z)T_B(-\mu', z)d\mu'. \quad (5)$$

The boundary condition at $z = 0$ corresponds to scattering from a rough surface having thermodynamic temperature T_s

$$\mu T_B(\mu, 0) = \int_0^1 s(\mu, \mu')T_B(-\mu', 0)d\mu' + \left(\mu - \int_0^1 s(\mu', \mu)d\mu' \right) T_s, \quad (\mu > 0). \quad (6)$$

Here, $s(\mu, \mu')$ is the surface bistatic scattering matrix. As in the case of p , the surface function s is an azimuthally averaged scattering cross section per unit surface area. For the natural case of reciprocal media, we note that the scattering function is symmetric: $s(\mu, \mu') = s(\mu', \mu)$. We assume for simplicity that polarizations are uncoupled by both surface and hydrometeor scattering. Finally, at the topmost atmospheric level $z = H$, the downward propagating cosmic background radiation temperature is

$$T_B(-\mu, H) = T_{cb} = 2.73 \text{ K}. \quad (7)$$

Equation (7) can be easily modified to model the small galactic radiation contribution. In the above formulation, we have implicitly assumed the Rayleigh–Jeans approximation, although doing so does not restrict the solution since the full Planck function can be substituted in place of $T_{\text{atm}}(z)$, T_s , and T_{cb} .

Discretizing the DRTE over a set of quadrature angles θ_i [31] results in the following set of angularly coupled equations:

$$\begin{aligned} \mu_i \frac{dT_i^+}{dz} &= -\kappa_e T_i^+ + \kappa_a T_{\text{atm}} + \kappa_s \\ &\quad \cdot \left[\sum_{j=1}^M \gamma_j P_{ij}^{++} T_j^+ + \sum_{j=1}^M \gamma_j P_{ij}^{+-} T_j^- \right] \\ -\mu_i \frac{dT_i^-}{dz} &= -\kappa_e T_i^- + \kappa_a T_{\text{atm}} + \kappa_s \\ &\quad \cdot \left[\sum_{j=1}^M \gamma_j P_{ij}^{-+} T_j^+ + \sum_{j=1}^M \gamma_j P_{ij}^{--} T_j^- \right] \end{aligned} \quad (8)$$

where $\mu_i = \cos \theta_i$ and M is the number of quadrature angles between zenith and the horizon (i.e., the number of upward or downward propagating streams). Here, we have

$$\begin{aligned} P_{ij}^{++} &= p(\mu_i, \mu_j) \\ P_{ij}^{+-} &= p(\mu_i, -\mu_j) \\ P_{ij}^{-+} &= p(-\mu_i, \mu_j) \\ P_{ij}^{--} &= p(-\mu_i, -\mu_j) \end{aligned} \quad (9)$$

and the γ_j are appropriate positive quadrature weights. Optimally, the γ_j are selected to be the Christoffel weights [32] to implement Gauss–Legendre quadrature, although in principal any quadrature scheme can be used. In the above discrete ordinate approach, we have separated the up- and downwelling components of radiation (T_j^+ and T_j^- , respectively), and all μ_i are positive. According to Kirchhoff's law for reciprocal media, the discretized scattering matrix P is symmetric with respect to simultaneous permutation of angular indexes

$$P_{ij}^{++} = P_{ji}^{++} \quad P_{ij}^{--} = P_{ji}^{--} \quad P_{ij}^{-+} = P_{ji}^{+-}. \quad (10)$$

We will assume also that the hydrometeor absorption and scattering properties are invariant with respect to up/down propagation, in which case

$$P_{ij}^{++} = P_{ij}^{--} \quad P_{ij}^{-+} = P_{ij}^{+-}. \quad (11)$$

Thus, the phase function is symmetric with respect to independent permutations of both upper and lower indexes. Using the Henyey–Greenstein phase matrix we can take scattering asymmetry into account through the asymmetry parameter g

$$\begin{aligned} P_{i,j}^{\sigma_1 \sigma_2} &= \frac{1-g^2}{2\pi} \int_{-\pi}^{\pi} (1+g^2 - 2\sigma_1 \sigma_2 g \mu_i \mu_j \\ &\quad + 2g \sqrt{1-\mu_i^2} \sqrt{1-\mu_j^2} \cos t)^{-\frac{3}{2}} dt \end{aligned} \quad (12)$$

where $\sigma_{1,2} = \pm 1$. Finally, boundary conditions for the discretized equations are

$$\begin{aligned} \mu_i T_i^+ &= \sum_{j=1}^M \gamma_j s_{ij} T_j^- + \left(\mu_i - \sum_{j=1}^M \gamma_j s_{ji} \right) T_s \quad (z=0) \\ T_i^- &= T_{cb} \quad (z=H) \end{aligned} \quad (13)$$

and in the case of a specular surface, we have

$$s_{ij} = \mu_i |R_i|^2 \delta_{ij}, \quad \gamma_j = 1 \quad (14)$$

where R_i is the Fresnel reflection coefficient for the corresponding angle.

Symmetry properties of (8) are very significant to our approach. Following [33], to make the equations explicitly symmetric, we introduce new variables for the upwelling and downwelling streams as follows:

$$u_i = \sqrt{\mu_i \gamma_i} T_i^+ \quad v_i = \sqrt{\mu_i \gamma_i} T_i^-. \quad (15)$$

Now, (8) takes the following form:

$$\begin{aligned}\frac{du_i}{dz} &= -\sum_{j=1}^M A_{0ij}u_j - \sum_{j=1}^M B_{0ij}v_j + f_i \\ \frac{dv_i}{dz} &= \sum_{j=1}^M B_{0ij}u_j + \sum_{j=1}^M A_{0ij}v_j - f_i\end{aligned}\quad (16)$$

where

$$A_{0ij} = \frac{1}{\mu_i} \kappa_e \delta_{ij} - \kappa_s \sqrt{\frac{\gamma_i \gamma_j}{\mu_i \mu_j}} P_{ij}^{++} \quad (17)$$

$$B_{0ij} = -\kappa_s \sqrt{\frac{\gamma_i \gamma_j}{\mu_i \mu_j}} P_{ij}^{+-} \quad (18)$$

$$f_i = \sqrt{\frac{\gamma_i}{\mu_i}} \kappa_a T_{\text{atm}}. \quad (19)$$

The boundary condition at the surface becomes

$$u_i = \sum_{j=1}^M S_{ij}v_j + f_i^{(0)} \quad (z=0) \quad (20)$$

where

$$S_{ij} = \sqrt{\frac{\gamma_i \gamma_j}{\mu_i \mu_j}} s_{ij} \quad (21)$$

and

$$f_i^{(0)} = \sqrt{\frac{\gamma_i}{\mu_i}} \left(\mu_i - \sum_{j=1}^M \gamma_j s_{ji} \right) T_s \quad (22)$$

and the boundary condition at the top of the atmosphere becomes

$$v_i = f_i^{(N+1)} = \sqrt{\gamma_i \mu_i} T_{cb} \quad (z=H). \quad (23)$$

The vector quantities f , $f^{(0)}$, and $f^{(N+1)}$ represent sources due to atmospheric, surface, and cosmic background radiation, respectively. Equations (16) with boundary conditions (20) and (23) thus represent the problem to be solved.

It is important in our approach that the matrices $A_0 + B_0$ and $A_0 - B_0$ are both symmetric and positive semidefinite, a condition which immediately follows from Gershgorin's circle theorem and noting that $\kappa_e \geq \kappa_s$. To illustrate its application we reproduce the argument. Let λ , u_i be an eigenvalue and the corresponding eigenvector of the following symmetric matrix, which is part of the matrix $A_0 + B_0$:

$$\sum_{j=1}^M \left[\frac{1}{\mu_i} \sum_{k=1}^M \gamma_k (P_{ki}^{++} + P_{ki}^{+-}) \delta_{ij} - \sqrt{\frac{\gamma_i \gamma_j}{\mu_i \mu_j}} (P_{ij}^{++} + P_{ij}^{+-}) \right] u_j = \lambda u_i \quad (24)$$

and let i_0 be an index corresponding to the maximal value of the ratio $u_i/\sqrt{\mu_i \gamma_i}$, that is $|u_{i_0}/\sqrt{\mu_{i_0} \gamma_{i_0}}| \geq u_i/\sqrt{\mu_i \gamma_i}$ for all

i . Since an eigenvector is defined to within an arbitrary multiplying factor, we can assume that $u_{i_0} > 0$. It thus follows that

$$\begin{aligned}\lambda u_{i_0} &= \frac{u_{i_0}}{\mu_{i_0}} \sum_{k=1}^M \gamma_k (P_{ki_0}^{++} + P_{ki_0}^{+-}) \\ &\quad - \sum_{j=1}^M \sqrt{\frac{\gamma_{i_0} \gamma_j}{\mu_{i_0} \mu_j}} (P_{i_0j}^{++} + P_{i_0j}^{+-}) u_j \\ &\geq \frac{u_{i_0}}{\mu_{i_0}} \sum_{k=1}^M \gamma_k (P_{ki_0}^{++} + P_{ki_0}^{+-}) \\ &\quad - \sqrt{\frac{\gamma_{i_0}}{\mu_{i_0}}} \frac{u_{i_0}}{\sqrt{\mu_{i_0} \gamma_{i_0}}} \sum_{j=1}^M \gamma_j (P_{i_0j}^{++} + P_{i_0j}^{+-}) \\ &= 0\end{aligned}\quad (25)$$

where the symmetry and nonnegativeness of the entries of the phase matrix P were used. The remainder of the matrix $A_0 + B_0$ which is not accounted for in (24) represents a diagonal matrix with positive entries proportional to the total (gaseous and hydrometeor) absorption. Thus, the matrix $A_0 + B_0$ is, in general, positive semidefinite and positive definite in the presence of some gas and/or hydrometeor absorption. The same argument can be applied to the case of the matrix $A_0 - B_0$.

III. REFLECTION AND TRANSMISSION OPERATORS FOR A SINGLE LAYER

To solve the discrete ordinate system, we represent the atmosphere as a stack of homogeneous layers within which the medium properties (matrices A_0 , B_0 , and f) are assumed constant. The layers are not necessarily thin, and brightness temperature can change greatly within a layer. Thus, the method is accurate even in many practical cases where a layer may be nearly opaque. The overall solution subsequently uses the adding method (e.g., [34]) in a recursion to calculate the properties of a stack of layers by adding one layer to the stack at a time. This approach allows not only robust and quick calculation of the brightness temperature profile itself, but also fast calculation of the radiation Jacobian \overline{H}_R .

To proceed, we describe solutions for the reflection and transmission matrices (r and t) for a single layer embedded in vacuum between levels $z = 0$ and $z = h$. Here and below, all values characterizing radiation field solutions are assumed to be vectors of length M , with one entry for each angle. We assume an external radiation field u_{inc} incident on the layer from below for which the reflected and transmitted fields v and u at $z = 0$ and $z = h$, respectively, are described by (Fig. 1)

$$v = r u_{\text{inc}} \text{ at } z = 0 \quad (26)$$

$$u = t u_{\text{inc}} \text{ at } z = h. \quad (27)$$

As a result of assumed mirror symmetry of the layer, the same matrices r and t will also describe the upward and downward propagating fields at the top and bottom of the layer caused by external radiation incident from above. The matrices r and t are

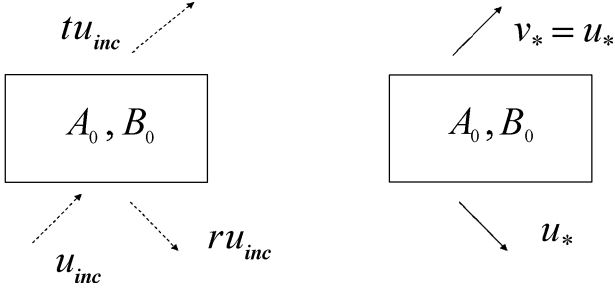


Fig. 1. Calculation of the reflection and transmission operators and self-radiation field for a single layer.

independent of internal sources (described in (16) by f) and are related to the solutions of the homogeneous coupled DRTE

$$\frac{d}{dz} \begin{pmatrix} u \\ v \end{pmatrix} = \begin{pmatrix} -A_0 & -B_0 \\ B_0 & A_0 \end{pmatrix} \begin{pmatrix} u \\ v \end{pmatrix}. \quad (28)$$

The above system¹ is governed only by matrices A_0 and B_0 . The general solution of (28) can be represented as follows:

$$\begin{pmatrix} u(z) \\ v(z) \end{pmatrix} = \frac{1}{2} \begin{pmatrix} 1 & 1 \\ -1 & 1 \end{pmatrix} \begin{pmatrix} c & -sA \\ -Bs & c^T \end{pmatrix} \cdot \begin{pmatrix} 1 & -1 \\ 1 & 1 \end{pmatrix} \begin{pmatrix} u(0) \\ v(0) \end{pmatrix} \quad (29)$$

where

$$\begin{aligned} A &\triangleq A_0 + B_0 \\ B &\triangleq A_0 - B_0 \end{aligned} \quad (30)$$

and the following matrix functions have been introduced:

$$\begin{aligned} c &\triangleq \cosh(\sqrt{AB}z) \\ s &\triangleq \sinh(\sqrt{AB}z) \cdot (AB)^{-\frac{1}{2}}. \end{aligned} \quad (31)$$

The simplest way to ensure that (29) is a solution of (28) is by direct substitution and making use of the following matrix identity:

$$Bg(AB) = g(BA)B \quad (32)$$

where g is an arbitrary matrix function. (This identity is obvious for integer powers $g = x^n$ and, thus, holds for any analytic matrix function.)

We can now express the matrices r and t in terms of A and B . The field at $z = 0$ is $u = u_{\text{inc}}$ and $v = ru_{\text{inc}}$, and at $z = h$ it is $u = tu_{\text{inc}}$, and $v = 0$. Substituting these values into relation (29), we find

$$\begin{pmatrix} tu_{\text{inc}} \\ 0 \end{pmatrix} = \frac{1}{2} \begin{pmatrix} 1 & 1 \\ -1 & 1 \end{pmatrix} \begin{pmatrix} c & -sA \\ -Bs & c^T \end{pmatrix} \cdot \begin{pmatrix} 1 & -1 \\ 1 & 1 \end{pmatrix} \begin{pmatrix} u_{\text{inc}} \\ ru_{\text{inc}} \end{pmatrix} \quad (33)$$

¹Note that (28) coincides with [28, eq. (78)] with the important difference being that our submatrices A_0 and B_0 are symmetric.

where the matrices c and s are calculated at $z = h$. Carrying out the matrix multiplications and considering the second row of the system yields

$$(c + c^T + sA + Bs)ru_{\text{inc}} = (c - c^T - sA + Bs)u_{\text{inc}} \quad (34)$$

from which we find the reflection matrix

$$r = (c + c^T + sA + Bs)^{-1}(c - c^T - sA + Bs). \quad (35)$$

To obtain a similar expression for t , we first rewrite (33) as

$$\frac{1}{2} \begin{pmatrix} 1 & 1 \\ -1 & 1 \end{pmatrix} \begin{pmatrix} c & sA \\ Bs & c^T \end{pmatrix} \begin{pmatrix} 1 & -1 \\ 1 & 1 \end{pmatrix} \begin{pmatrix} tu_{\text{inc}} \\ 0 \end{pmatrix} = \begin{pmatrix} u_{\text{inc}} \\ ru_{\text{inc}} \end{pmatrix}. \quad (36)$$

One can ascertain this identity by direct calculation. Equivalently, (36) follows immediately from (33) by noting that according to symmetry the inverse of the hyperbolic matrix becomes

$$\begin{aligned} \begin{pmatrix} c & -sA \\ -Bs & c^T \end{pmatrix}^{-1} (z) &= \begin{pmatrix} c & -sA \\ -Bs & c^T \end{pmatrix} (-z) \\ &= \begin{pmatrix} c & sA \\ Bs & c^T \end{pmatrix} (z). \end{aligned} \quad (37)$$

Following the general procedure used to find r , we can solve (36) for the transmission matrix

$$t = 2(c + c^T + sA + Bs)^{-1}. \quad (38)$$

Owing to thermal emission, the layer will also generate at its upper surface an upward propagating radiation field, which we denote as $u(h) = u_*$. Due to mirror symmetry of the layer, the downward propagating thermal radiation field at $z = 0$ will be also equal to u_* , i.e., $v_* = v(0) = u_*$. The general solution of the inhomogeneous equation

$$\frac{d}{dz} \begin{pmatrix} u \\ v \end{pmatrix} = \begin{pmatrix} -A_0 & -B_0 \\ B_0 & A_0 \end{pmatrix} \begin{pmatrix} u \\ v \end{pmatrix} + \begin{pmatrix} f \\ -f \end{pmatrix} \quad (39)$$

can (by inspection) be represented as the sum of a constant (z -independent) vector

$$\begin{pmatrix} u_{\text{inh}} \\ v_{\text{inh}} \end{pmatrix} = \begin{pmatrix} A^{-1}f \\ A^{-1}f \end{pmatrix} \quad (40)$$

superposed on any solution of the homogeneous equation (28). The particular solution describing the self-radiation of the layer should have an upwelling component that vanishes at $z = 0$ and a downwelling component that vanishes at $z = h$. By adding an artificial external component of radiation $u = -u_{\text{inh}}$ incident onto the layer from below we compensate the upwelling component of the upwelling propagating field at the top of the layer equal to $-tu_{\text{inh}}$. Similarly, an artificial external component of radiation $v = -u_{\text{inh}}$ incident onto the layer from above will compensate the downwelling component v_{inh} at the top $z = h$. In turn, this added field will produce an additional component of the upwelling propagating field at the top of the layer equal

to $-ru_{\text{inh}}$. Adding these contributions results in an expression for the thermally emitted field in terms of matrices r and t

$$u_* = u_{\text{inh}} - tu_{\text{inh}} - ru_{\text{inh}} = (1 - r - t)A^{-1}f. \quad (41)$$

Physically, we interpret the term $(1 - r - t)$ as an effective emissivity matrix for the layer, with the remaining terms proportional to the layer temperature and related dimensionless factors. It can be easily proven that the matrices r and t are both symmetric.

IV. CALCULATION OF EXPONENTIAL OPERATORS

For the case of a general atmosphere, we need to be able to accurately calculate functions of the matrix operators entering (35) and (38). For sufficiently small matrices Ah and/or Bh (so that the geometric mean product $\sqrt{AB}h$ is small), one can directly apply Taylor expansions

$$\begin{aligned} c &= \cosh(\sqrt{AB}h) \\ &= 1 + \frac{(AB)}{2!}h^2 + \frac{(AB)^2}{4!}h^4 + \dots \end{aligned} \quad (42)$$

$$\begin{aligned} s &= \sinh(\sqrt{AB}h) \cdot (AB)^{-\frac{1}{2}} \\ &= h + \frac{(AB)}{3!}h^3 + \frac{(AB)^2}{5!}h^5 + \dots \end{aligned} \quad (43)$$

In the general case, however, the above expansions require too many terms for practical and accurate implementation. A universal means to calculate a matrix function is first to transform it into a diagonal form. In our procedure, this problem is greatly simplified by the fact that the matrices A and B are symmetric and positively definite. Since A is symmetric, it can be represented as follows:

$$A = M_1 \Lambda_1 M_1^T \quad (44)$$

where M_1 is an orthogonal matrix consisting of eigenvectors of the symmetric matrix A

$$M_1 M_1^T = I \quad (45)$$

and Λ_1 is a diagonal matrix of associated eigenvalues. Since A is symmetric, all of its eigenvalues are guaranteed to be real, and since A is positive definite, these eigenvalues are nonnegative. Next, we define a second symmetric matrix $\Lambda_1^{1/2} M_1^T B M_1 \Lambda_1^{1/2}$. This matrix is also positive definite, since all entries of $\Lambda_1^{1/2}$ are real and nonnegative, and the matrix B is positive definite. Thus, this matrix can also be represented in diagonal form with the help of another orthogonal matrix M_2

$$\Lambda_1^{1/2} M_1^T B M_1 \Lambda_1^{1/2} = M_2 \Lambda_2 M_2^T \quad (46)$$

where the matrix Λ_2 is a diagonal matrix of associated nonnegative eigenvalues. Using (45) and (46), the product AB can be represented as

$$AB = \left(M_1 \Lambda_1^{1/2} M_2 \right) \Lambda_2 \left(M_1 \Lambda_1^{-1/2} M_2 \right)^T. \quad (47)$$

This is, in fact, a diagonal representation of the matrix AB , since

$$\left(M_1 \Lambda_1^{-1/2} M_2 \right)^T = \left(M_1 \Lambda_1^{1/2} M_2 \right)^{-1}. \quad (48)$$

As a result, any arbitrary analytic function g of the matrix AB can be calculated as follows:

$$g(AB) = \left(M_1 \Lambda_1^{1/2} M_2 \right) g(\Lambda_2) \left(M_1 \Lambda_1^{-1/2} M_2 \right)^T. \quad (49)$$

For the general case, the only nontrivial operation associated with the calculation of matrices c and s is, thus, a diagonalization of two real symmetric matrices. This operation is amenable to very effective standard numerical procedures.

V. STABLE CALCULATION OF REFLECTION AND TRANSMISSION OPERATORS

Equation (49) solves the problem of calculating the matrix operators c and s . Subsequently, the matrices r and t can be obtained by inversion of the matrix

$$P = c + c^T + sA + Bs \quad (50)$$

and substitution into (35) and (38). Although analytically correct, this procedure cannot be blindly applied in practice, especially for nontransparent layers. The problem is that for significantly opaque layers, the matrix functions c and s contain fast growing exponentials that quickly lead to numerical overflow. Simple extraction of the fastest growing exponential factor from the matrix P does not help, as we shall discuss shortly. This problem manifests itself as a well-known instability associated with implementation of the discrete ordinate method (e.g., see [28]).

To circumvent this problem, we need to look closer at the structure of P . Using the expansions in (44) and (47) along with the orthogonality relation (45) (which holds for the orthogonal matrix M_2 as well), one can check by direct calculation that P can be represented in the following form:

$$P = M_1 a \zeta b_t M_1^T \quad (51)$$

where

$$a = \Lambda_1^{1/2} M_2 + \Lambda_1^{-1/2} M_2 \Lambda_2^{1/2} \coth \left(\frac{1}{2} \Lambda_2^{1/2} h \right) \quad (52)$$

$$b_t = M_2^T \Lambda_1^{1/2} + \Lambda_2^{1/2} \tanh \left(\frac{1}{2} \Lambda_2^{1/2} h \right) M_2^T \Lambda_1^{-1/2} \quad (53)$$

and

$$\zeta = \Lambda_2^{-1/2} \sinh \left(\Lambda_2^{1/2} h \right). \quad (54)$$

Similarly, one can represent the other matrix factor entering (35) as

$$c - c^T - sA + Bs = 2 - M_1 a \zeta b_r M_1^T \quad (55)$$

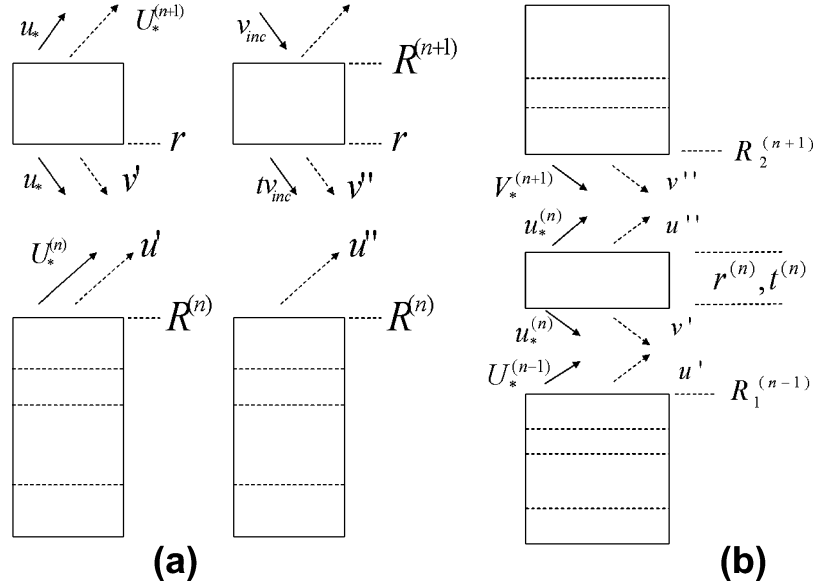


Fig. 2. Illustration of the derivation of recursion relations for (a) upward marching and (b) property variations within a single layer.

where

$$b_r = M_2^T \Lambda_1^{\frac{1}{2}} - \Lambda_2^{\frac{1}{2}} \tanh\left(\frac{1}{2} \Lambda_2^{\frac{1}{2}} h\right) M_2^T \Lambda_1^{-\frac{1}{2}}. \quad (56)$$

Note that the matrices associated with the hyperbolic functions in (52)–(54) and (56) are all diagonal; thus, their calculation is straightforward. Using the factorizations in (51) and (55), we obtain the following compact expressions for the reflection and transmission matrices r and t for a single layer:

$$t = 2P^{-1} = 2M_1 b_t^{-1} \zeta^{-1} a^{-1} M_1^T \quad (57)$$

$$r = P^{-1}(c - c^T - sA + Bs) = t - M_1 b_t^{-1} b_r M_1^T. \quad (58)$$

In contrast to the original expressions in (35) and (38), the representations in (57) and (58) remain numerically bounded in the limit $h \rightarrow \infty$. In this case, the matrices a , b_t , and b_r tend to finite limits, since $\tanh(\sqrt{\lambda_{2k}} h/2) \rightarrow 1$. Simultaneously, the values ζ_k^{-1} become exponentially small, and according to (57), the transmission matrix tends exponentially to zero as would be expected physically. Meanwhile the reflection operator r tends to a fixed limit, since the diagonal matrix ζ does not influence (58).

Equation (51) reveals why direct inversion of P given by (50) fails for sufficiently opaque layers. In this case, the condition number of the matrix P is determined primarily by the condition number of the matrix ζ , which grows exponentially with layer thickness. In other words, for thick layers, the matrix ζ is dominated by its largest entry, which according to (54) corresponds to the maximal eigenvalue λ_{2k} . Due to limited representational accuracy, this eigenvalue effectively nullifies the impact of all other eigenvalues of ζ . Thus, the matrix P effectively becomes singular, and if calculated according to (50), it cannot be numerically inverted.

On the other hand, explicit inversion according to (57) will always work. In fact, the larger the value of λ_{2k} , the less will be its contribution to P^{-1} , and the more that the operator $t =$

$2P^{-1}$ will be determined by the smallest value of λ_{2k} . This eigenvalue corresponds to the angular radiation mode with the least attenuation through the layer.

VI. SOLUTION FOR MULTIPLE LAYERS

Let us now consider a stack consisting of n layers. We denote the vector of emitted thermal radiation at the top of the stack as $U_*^{(n)}$. The reflection matrix $R^{(n)}$ is similarly defined with reference to a single layer as a matrix that transforms the downwelling component of the radiation field v_{inc} incident on the stack from above into an associated upward propagating field u

$$u = R^{(n)} v_{\text{inc}}. \quad (59)$$

For clarity, we use uppercase characters to denote a stack of layers and lowercase characters to denote an individual layer. Let us assume that an extra $(n+1)$ th layer with matrices r , t , and u_* is to be added to the top of an existing stack of n layers. At the boundary between the top of the stack and an extra layer, there will be present thermal radiation fields $U_*^{(n)}$ (upwelling) and $v_* = u_*$ (downwelling) along with additional fields u' and v' due to multiple reflections of the thermal fields from the extra layer and the stack. Thus, the total upwelling and downwelling components of radiation at the boundary will be equal to $U_*^{(n)} + u'$ and $u_* + v'$, respectively [Fig. 2(a)].

According to the definitions of the operators $R^{(n)}$ and r , one thus obtains

$$u' = R^{(n)}(u_* + v') \quad (60)$$

$$v' = r(U_*^{(n)} + u'). \quad (61)$$

The thermal field $U_*^{(n+1)}$ at the top of an extra layer (i.e., of the extended stack) will be

$$U_*^{(n+1)} = u_* + t(U_*^{(n)} + u'). \quad (62)$$

Equations (60) and (61) can be easily solved to obtain

$$U_*^{(n+1)} = u_* + t \left(1 - R^{(n)}r\right)^{-1} \left(U_*^{(n)} + R^{(n)}u_*\right). \quad (63)$$

Similarly, if an external downwelling field v_{inc} is incident on the top of the extended stack, this will result in the presence at the boundary between the initial stack and the extra layer two additional up- and downwelling fields u'' and v'' . Those fields must satisfy the following equations:

$$u'' = R^{(n)}v'' \quad (64)$$

$$v'' = ru'' + tv_{\text{inc}}. \quad (65)$$

The upwelling components of the field due to v_{inc} at the top of the extended stack, which by definition is equal to $R^{(n+1)}v_{\text{inc}}$, can be expressed as follows:

$$R^{(n+1)}v_{\text{inc}} = rv_{\text{inc}} + tu''. \quad (66)$$

Solving (64) and (65) and substituting the result into (66), we obtain

$$R^{(n+1)} = r + t \left(1 - R^{(n)}r\right)^{-1} R^{(n)}t. \quad (67)$$

Note that the reflection matrix values are constrained to be less than unity, provided that some absorption is present. It, thus, follows that the matrix $1 - R^{(n)}r$ is nonsingular, and hence invertible. The opposite would imply the presence of trapped radiation “modes” that could exist within the stack even without external sources of radiation. It is straightforward to show that all matrices $R^{(n)}$ are symmetric.

Once the r and t matrices for all individual layers are known, (63) and (67) provide a means for recurrent calculation of the thermal radiation field U_* and overall reflection matrix R by combining layers starting from the bottom $z = 0$ to the top $z = h$. At the bottom, the initial conditions are given by the boundary condition in (20)

$$U_*^{(0)} = f^{(0)} \quad (68)$$

and

$$R^{(0)} = S \quad (69)$$

where S is defined in (21). Once the operator $R^{(N)}$ at the top of the stack is reached, we calculate components of the field at the top by

$$v^{(N)} = f^{(N+1)} \quad (70)$$

$$u^{(N)} = U_*^{(N)} + R^{(N)}v^{(N)}. \quad (71)$$

The fields at the boundaries between layers can now be calculated by downward recursion. If the fields at the top of the n th layer are $u^{(n)}$ and $v^{(n)}$, and those at the bottom of the n th layer are $u^{(n-1)}$ and $v^{(n-1)}$, then the following relations hold:

$$u^{(n-1)} = R^{(n-1)}v^{(n-1)} + U_*^{(n-1)} \quad (72)$$

$$v^{(n-1)} = ru^{(n-1)} + tv^{(n)} + u_* \quad (73)$$

where r and t are reflection and transmission operators, and u_* is the self-radiation field of the n th layer. A recursive solution of these equations is as follows:

$$v^{(n-1)} = \left(1 - rR^{(n-1)}\right)^{-1} \left(rU_*^{(n-1)} + tv^{(n)} + u_*\right) \quad (74)$$

$$u^{(n-1)} = R^{(n-1)}v^{(n-1)} + U_*^{(n-1)}. \quad (75)$$

Using (74) and (75), one can proceed to compute the fields at each boundary between the layers from the top to the bottom of the stack. If necessary, one can also calculate the fields within each layer using (29). The number of operations required using this algorithm is, thus, directly proportional to total number of layers N .

VII. RADIATION JACOBIAN SOLUTION

The rows of the Jacobian $\overline{\overline{H}}$ are the incremental brightness sensitivity profiles (e.g., [35]) that are essential for both retrievals and radiance assimilation. These profiles require calculation of $\overline{\overline{H}}_R$, the derivatives of the brightness field at some fixed altitude and angle with respect to all radiative parameters of the atmosphere, specifically

$$\frac{\partial T_B(\theta, z)}{\partial \beta_n}, \quad n = 0, 1, \dots, N \quad (76)$$

where the parameter β_n is either κ_s , κ_a , T_{atm} , or g for the n th level. For simplicity, we assume the observation level z to coincide with one of the boundaries $n_{\text{obs}} = 0, 1, \dots, N$ between the layers (e.g., $n_{\text{obs}} = N$ for satellite-based observations).

Although the approach presented in the previous section can be used to calculate $\overline{\overline{H}}_R$, straightforward application can lead to a relatively inefficient algorithm. The reason for the inefficiency is that variations of the parameters characterizing the radiative properties of any specific layer (i.e., matrices A_0 , B_0 and source f for some value of n) will result in variations of the reflection operators and self-radiation fields for all stacks that contain this layer. Accordingly, a complete upward and downward recursion is required to be repeated for variations within each successive layer. In this case, the total number of operations required will be proportional to N^2 , and not N . For this reason, we slightly modify our approach to calculate $\overline{\overline{H}}_R$.

Recall first that during upward recursion, we calculated and stored all reflection operators $R^{(n)}$ and upwelling self-radiation fields $U_*^{(n)}$, $n = 0, 1, \dots, N$. In this section, we modify our notation for these reflection operators by denoting them as $R_1^{(n)}$. Now, using the same (63) and (67), we calculate during downward recursions similar reflection operators $R_2^{(n)}$ and downwelling self-radiation fields $V_*^{(n)}$ for stacks of layers that include the n th layer and all layers above it. Initial conditions for this recursion are $R_2^{(N)} = 0$ and $V_*^{(N)} = f^{(N+1)}$. Thus, if an external field u_{inc} is incident onto the stack of layers from below, then $v = R_2^{(n)}u_{\text{inc}}$ will represent the reflected downward propagating field, and $V_*^{(n)}$ will represent the downwelling self-radiation at the bottom of each upper stack (i.e., the bottom of the n th layer). Note that the number of layer operations required for the calculation of all these values is still proportional to N .

Consider the brightness variation with respect to any radiative parameter β_n within a specific (n th) layer, where $n = 1, 2, \dots, N$. At the top of this layer will be present downwelling self-radiation from the upper stack $V_*^{(n+1)}$ and upwelling self-radiation from the layer $u_*^{(n)}$. Similarly, at the bottom of the layer will be present downwelling self-radiation from the layer $v_*^{(n)} = u_*^{(n)}$ and upwelling self-radiation from the lower stack $U_*^{(n-1)}$. As a result of the interaction of the radiation fields within the stacks and the n th layer, at the bottom of this layer will appear additional upward and downward propagating fields, denoted as u' , v' , respectively. Similarly, at the top of the n th layer will appear additional fields, denoted as u'' , v'' [Fig. 2(b)]. As in the previous section, using definitions of the reflection and transmission operators, we obtain the following equations for these additional fields:

$$u' = R_1^{(n-1)} (v' + u_*^{(n)}) \quad (77)$$

$$v'' = R_2^{(n+1)} (u'' + u_*^{(n)}) \quad (78)$$

$$u'' = r^{(n)} (v'' + V_*^{(n+1)}) + t^{(n)} (u' + U_*^{(n-1)}) \quad (79)$$

$$v' = t^{(n)} (v'' + V_*^{(n+1)}) + r^{(n)} (u' + U_*^{(n-1)}). \quad (80)$$

These equations can be easily solved. Substituting (77) and (78) into (79) and (80), we obtain

$$a_{11}u'' + a_{12}v' = b_1 \quad (81)$$

$$a_{21}u'' + a_{22}v' = b_2 \quad (82)$$

where

$$\begin{aligned} a_{11} &= 1 - r^{(n)} R_2^{(n+1)} & a_{12} &= -t^{(n)} R_1^{(n-1)} \\ a_{21} &= -t^{(n)} R_2^{(n+1)} & a_{22} &= 1 - r^{(n)} R_1^{(n-1)} \end{aligned} \quad (83)$$

and

$$b_1 = r^{(n)} (V_*^{(n+1)} + R_2^{(n+1)} u_*^{(n)}) + t^{(n)} (U_*^{(n-1)} + R_1^{(n-1)} u_*^{(n)}) \quad (84)$$

$$b_2 = t^{(n)} (V_*^{(n+1)} + R_2^{(n+1)} u_*^{(n)}) + r^{(n)} (U_*^{(n-1)} + R_1^{(n-1)} u_*^{(n)}). \quad (85)$$

From (81) and (82), we find

$$u'' = (a_{11} - a_{12}a_{22}^{-1}a_{21})^{-1} (b_1 - a_{12}a_{22}^{-1}b_2) \quad (86)$$

$$v' = (a_{22} - a_{21}a_{11}^{-1}a_{12})^{-1} (b_2 - a_{21}a_{11}^{-1}b_1). \quad (87)$$

Similar expressions for u' and v'' follow after substitution of (86) and (87) into (77) and (78).

An important advantage of this form of solution is that variation of the radiative parameters at the n th layer leads only to variations of $r^{(n)}$, $t^{(n)}$, and $u_*^{(n)}$, with no effect on $R_1^{(n-1)}$, $R_2^{(n+1)}$, $U_*^{(n-1)}$, and $V_*^{(n+1)}$. Let us denote the derivative with

respect to any radiative parameter β_n by a dot. Once β_n is specified, the values \dot{A}_n , \dot{B}_n , \dot{f}_n follow explicitly, as do the values $\dot{r}^{(n)}$, $\dot{t}^{(n)}$, and $\dot{u}_*^{(n)}$ for all layers $n = 1, 2, \dots, N$. Now, expressions for \dot{a}_{ij} and \dot{b}_i immediately follow from (83)–(85)

$$\begin{aligned} \dot{a}_{11} &= -\dot{r}^{(n)} R_2^{(n+1)} \\ \dot{a}_{12} &= -\dot{t}^{(n)} R_1^{(n-1)} \\ \dot{a}_{21} &= -\dot{t}^{(n)} R_2^{(n+1)} \\ \dot{a}_{22} &= -\dot{r}^{(n)} R_1^{(n-1)} \end{aligned} \quad (88)$$

$$\begin{aligned} \dot{b}_1 &= \dot{r}^{(n)} (V_*^{(n+1)} + R_2^{(n+1)} u_*^{(n)}) + r^{(n)} R_2^{(n+1)} \dot{u}_*^{(n)} \\ &\quad + \dot{t}^{(n)} (U_*^{(n-1)} + R_1^{(n-1)} u_*^{(n)}) + t^{(n)} R_1^{(n-1)} \dot{u}_*^{(n)} \end{aligned} \quad (89)$$

$$\begin{aligned} \dot{b}_2 &= \dot{t}^{(n)} (V_*^{(n+1)} + R_2^{(n+1)} u_*^{(n)}) + t^{(n)} R_2^{(n+1)} \dot{u}_*^{(n)} \\ &\quad + \dot{r}^{(n)} (U_*^{(n-1)} + R_1^{(n-1)} u_*^{(n)}) + r^{(n)} R_1^{(n-1)} \dot{u}_*^{(n)}. \end{aligned} \quad (90)$$

Expressions for \dot{u}' , \dot{v}' follow after differentiation of (86) and (87) (we skip the cumbersome result of this straightforward calculation). Finally, expressions for \dot{u}' and \dot{v}' follow upon differentiation of (77) and (78)

$$\dot{u}' = R_1^{(n-1)} (\dot{v}' + \dot{u}_*^{(n)}) \quad \dot{v}'' = R_2^{(n+1)} (\dot{u}'' + \dot{u}_*^{(n)}). \quad (91)$$

Calculation of the derivatives $\dot{r}^{(n)}$, $\dot{t}^{(n)}$, and $\dot{u}_*^{(n)}$ can be performed by direct differentiation of the explicit expressions in (57), (58), and (41). The only nontrivial operation here is differentiation with respect to the parameter matrices M_1 , M_2 , and Λ_1 , Λ_2 . However, this task is essentially equivalent to calculation of the first-order perturbations of the eigenvalues and eigenvectors of a symmetric matrix—a well-known procedure from quantum mechanics (e.g., [36]). In terms of our problem, the result can be stated as follows. Let a symmetric matrix η depending on some parameter β be represented in diagonal form

$$\eta = M \Lambda M^T \quad (92)$$

where $\Lambda = \text{diag}(\lambda_1, \dots, \lambda_M)$ is a diagonal matrix of eigenvalues, and M is an appropriate orthogonal matrix of eigenvectors. Both Λ and M depend on the parameter β . Then

$$\dot{\lambda}_n = (M^T \dot{\eta} M)_{nn} = \sum_{i,j} M_{in} \dot{\eta}_{ij} M_{jn} \quad (93)$$

and

$$\dot{M}_{nm} = \sum_{i \neq m} M_{ni} \frac{(M^T \dot{\eta}_{ij} M)_{im}}{\lambda_m - \lambda_i}. \quad (94)$$

Note that standard quantum-mechanical formulas correspond to the case where $M = 1$, i.e., the diagonal representation of the Hamiltonian.

The final operation is the calculation of the impact of the derivatives \dot{u}' , \dot{v}' , \dot{u}'' , and \dot{v}'' of the fields at each of $n = 1, 2, \dots, N$ levels at the observation level n_{obs} where the

radiometer is located. This recalculation can be done using (74) and (75) with the only difference being that the reflection and transmission operators r and t and self-radiation field u_* are replaced by the appropriate operators, and self-radiation fields corresponding not to a single layer, but rather to a stack of layers located between the current layer n and observation layer n_{obs} . These operators are also calculated recursively for all stream angles following the same pattern that was presented in the previous section, with the exception that the recursion now involves two different reflection and transmission operators that describe the cases for external radiation incident onto the stack from below and above, respectively. Note that for the case of a single layer, the operators coincide and are equal to r and t . In any case, the number of operations required to calculate the radiation Jacobian using this approach is still directly proportional to the total number of layers N .

VIII. NUMERICAL EXAMPLE

Geophysical features of the radiation Jacobian for a heavy scattering scenario are illustrated using calculations based on microphysical data from a numerical simulation of a hurricane. The simulation uses 6-km horizontal resolution and 60-level microphysical cloud data obtained from an MM5 model run for Hurricane Bonnie (August 26, 1998) [37]. Hydrometeor microphysical evolution is explicitly computed using the Reisner five-phase cloud model [12], [16]. Both brightness temperature fields and their derivatives with respect to the scattering and absorption coefficients and temperature were computed for a total of 74 500 profiles using $2M = 8$ radiation streams.

A nadir brightness map for a channel at 180.31 ± 17 GHz is shown in Fig. 3, along with cross-sectional cuts through the hurricane eyewall and rainbands at 33° latitude illustrating the radiative parameters [Fig. 3(b) and (c)] and the radiation Jacobian [Fig. 3(d)–(g)]. For purposes of illustration, we plotted the scaled derivatives $\partial T_B / \partial \ln \kappa_s = \kappa_s (\partial T_B / \partial \kappa_s)$ and $\partial T_B / \partial \ln \kappa_a = \kappa_a (\partial T_B / \partial \kappa_a)$ rather than the direct derivatives in the cross-sectional cuts. To account for the varying layer thicknesses, each Jacobian element is scaled by the inverse layer thickness $(z_n - z_{n-1})^{-1}$; thus, the dimensions are in units of kelvin per kilometer (K/km), except for $\partial T_B / \partial T_{\text{atm}}$, which is in units of per kilometer (km^{-1}).

From Fig. 3(d), we see that the Jacobian elements for variations in κ_s are always negative, since increases in scattering within the cloud tops increase the amount of reflection of the cold cosmic background temperature. Such large negative sensitivities are associated with most of the rainband and eyewall region, and extend several kilometers deep through the cloud-top ice layer down to the melting layer. Below the melting layer, the hydrometeors become liquid and no longer reflect as much due to both the opacity of the ice layer overhead and their liquid state.

While the sensitivity to κ_s is negative, Fig. 3(e) shows Jacobian elements for variations in κ_a that are either positive or negative in sign, explained as follows: over regions of weak scattering or surface reflection, any increase in absorption causes the altitude of maximum photon emission to ascend. Since the thermodynamic lapse rate is predominantly negative below the tropopause, the brightness temperature is thereby

reduced; hence, the Jacobian element is negative. However, over strong scattering or surface reflection, the brightness is dominated by cold reflection from the cosmic background, and any additional absorption reduces this reflectivity. Effectively, the reflecting cloud top (which could have up to $\sim 60\%$ reflectivity at certain millimeter wavelengths) or surface becomes a less reflective mirror, resulting in an increase in brightness temperature. Hence, the Jacobian element is positive over such layers. This bimodal behavior in the incremental response to absorption attests to the importance of accommodating scattering and surface reflection in microwave radiance assimilation methods.

Fig. 3(f) shows the Jacobian elements for scattering asymmetry g , which are always positive. Variations in g resulting from, for example, mean hydrometeor size changes, effectively vary the mean direction in which photons are scattered. An increase in g in the cloud top ice layer, for example, is associated with an increase in the percentage of photons that are scattered forward, and hence an effective reduction in scattering coefficient. Accordingly, the cloud top reflectivity is reduced and the brightness temperature increased. Although the impact of variations in g are smaller than those of other radiative parameters, neglect of asymmetry can result in errors of up to several tens of kelvins.

Finally, Fig. 3(g) shows the Jacobian elements for T_{atm} . At the extreme eastern edge of the cut, we see that the incremental response takes the familiar form of the clear-air temperature weighting function. As one proceeds westward into the rainbands and eyewall, the additional absorption from clouds and rain causes the temperature weighting function peak to ascend to higher altitudes. Profiles of extreme absorption have the peak lifted to the level of the clouds tops in the eyewall region.

IX. COMPLEXITY AND SPEED

As discussed, the number of operations required for calculation of both the brightness temperature profile and radiation Jacobian for all stream angles is directly proportional to the total number of layers N . With regard to the calculation of \overline{H}_R for NWP assimilation, this result cannot be taken for granted. The number of operations required for a discrete ordinate solution with a divided difference Jacobian is N^2 , and an iterative perturbation solution is N^3 . The algorithm also involves matrix operations such as matrix multiplications and matrix inversions as well as matrix diagonalizations, each of which requires a number of operations proportional to M^3 , where M is the total number of angles. Thus, the overall number of operations is proportional to NM^3 .

The algorithm presented in the previous sections was realized as a Fortran 90 computer code. The code was tested by comparing the left- and right-hand sides of (8) for test scattering atmospheres at 19.22 and 180.31 GHz. The results matched each other to the accuracy of the numerical differentiation with respect to z . It is also noted that inclusion of the radiation Jacobian calculation for derivatives with respect to κ_s , κ_a , g , and T_{atm} along with the brightness calculation increased the computation time by only a few percent, since calculation of the Jacobians uses many of the matrices required for calculation of T_B itself.

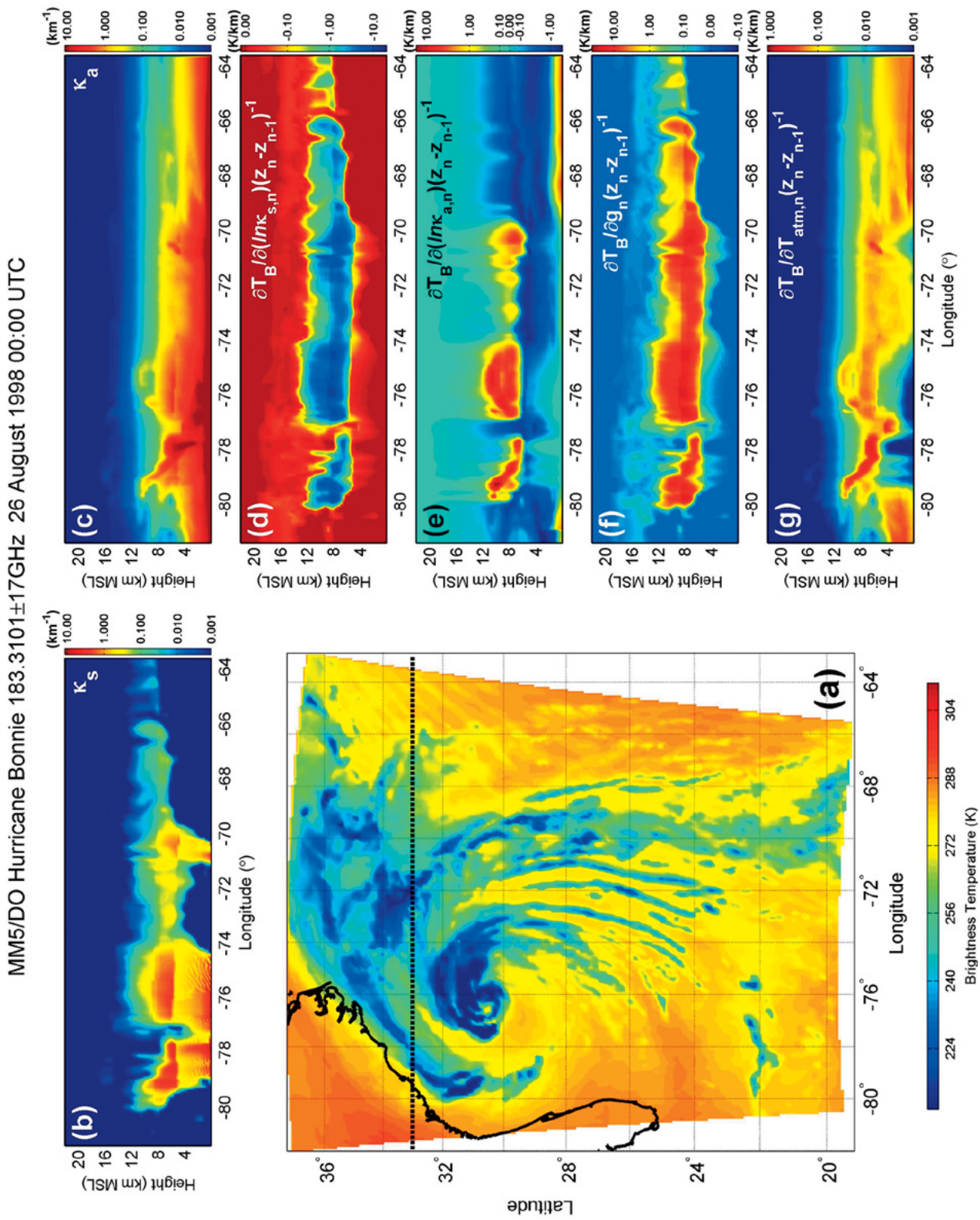


Fig. 3. Numerical results of the fast Jacobian algorithm at 183.31 ± 17 GHz for the Hurricane Bonnie simulation. (a) T_B map. (b) and (c) Cross-sectional cuts of radiation parameters κ_s and κ_a for 33° latitude, respectively. (d)–(g) Cross-sectional cuts of scaled radiation Jacobian values for parameters κ_s , κ_a , g , and T_{atm} for 33° latitude, respectively.

Absolute speed was assessed by considering the time required to perform brightness and Jacobian calculations on a test scattering atmosphere. For these tests, we used $N = 60$ levels and $2M = 8$ angles on a personal computer with a 1.81-GHz clock,² resulting in an average computation time of ~ 4.2 ms per profile. Using this performance as a baseline, we can scale this figure to assess performance in an operational environment. Considering that, on average, perhaps $\sim 10\%$ of a global profile set will exhibit significant scattering (which requires full-scale matrix operations versus trivial operations using diagonal matrices) an effective speed improvement of ~ 10 times relative to full global application can be applied. An additional factor of ~ 2 – 3 times was found when weakly scattering layers were approximated as nonscattering layers requiring only diagonal (versus full matrix) operations. Finally, use of a modern 2.8-GHz 128-processor parallel machine can be expected to provide an additional factor of ~ 200 times speed improvement. The resulting calculation time can, thus, be expected to be reduced to an average of ~ 1 μ s per profile channel. We can compare this figure to the profile rate expected to be required for assimilation of data from, e.g., the NPOESS CMIS sensor. For CMIS, pixels comprised of ~ 30 significant radiometric channels will be streamed every ~ 12 ms for a 10-km regridded product, resulting in a sample period of ~ 400 μ s per pixel-channel. Accordingly, the Jacobian technique permits a significant amount of idle time (~ 400 times) for related operations such as profile parameter preparation (to be addressed in a separate study), iteration, NWP model update, and related functions.

X. SUMMARY

We have presented herein a new multiple-stream discrete-ordinate algorithm for fast calculation of brightness temperatures and the associated radiation Jacobian for a plane-parallel atmosphere under arbitrary scattering and absorbing conditions. Unique features of the algorithm include inherent stability of the reflection and transmission matrix calculation and an efficient means of layer adding resulting in a Jacobian calculation of order NM^3 . Scaling calculations based on the performance of the algorithm on a standard personal computer suggest that the new algorithm will be suitable for use in real-time all-weather microwave radiance assimilation.

As a result of its inherent stability for all values of absorption and scattering, the RT solution presented herein can be used to compute the scattering-based Jacobian for any frequency. Adaptation to the IR and optical bands is easily performed by incorporating the full Planck function applied to all physical temperatures, at minimal computational expense. Extension of this approach to calculation of the two first Stokes parameters is straightforward, since appropriate scattering matrices possess the same fundamental symmetry properties as in the scalar case. Generalization of the technique to include surface and bistatic scattering effects is being pursued in a follow-on effort.

ACKNOWLEDGMENT

The authors are grateful to B. Stankov for help with the Jacobian renderings, J.-W. Bao for providing the Hurricane Bonnie MM5 data, and R. Hill for help in testing the routines.

REFERENCES

- [1] A. J. Gasiewski, "Numerical sensitivity analysis of passive EHF and SMMW channels to tropospheric water vapor, clouds, and precipitation," *IEEE Trans. Geosci. Remote Sensing*, vol. 30, pp. 859–870, Sept. 1992.
- [2] E. G. Njoku, W. J. Wilson, S. H. Yueh, and Y. Rahmat-Samii, "A large-antenna microwave radiometer-scatterometer concept for ocean salinity and soil moisture sensing," *IEEE Trans. Geosci. Remote Sensing*, vol. 38, pp. 2645–2655, Nov. 2000.
- [3] K. F. Evans, A. H. Evans, I. G. Nolt, and B. T. Marshall, "The prospect for remote sensing of cirrus clouds with a submillimeter-wave spectrometer," *J. Appl. Meteorol.*, vol. 38, pp. 514–525, 1999.
- [4] A. J. Gasiewski and J. T. Johnson, "Statistical temperature retrievals in clear-air using passive 118-GHz O₂ observations," *IEEE Trans. Geosci. Remote Sensing*, vol. 31, pp. 106–115, Jan. 1993.
- [5] J. G. Ferriday and S. K. Avery, "Passive microwave remote sensing of rainfall with SSM/I: Algorithm development and implementation," *J. Appl. Meteorol.*, vol. 33, pp. 1587–1596, Dec. 1994.
- [6] A. J. Gasiewski and D. H. Staelin, "Statistical precipitation cell parameter estimation using passive 118-GHz O₂ observations," *J. Geophys. Res.*, vol. 94, no. D15, pp. 18 367–18 378, Dec. 1989.
- [7] D. H. Staelin and F. W. Chen, "Precipitation observation near 54 and 183 GHz using the NOAA 15 satellite," *IEEE Trans. Geosci. Remote Sensing*, vol. 38, pp. 2322–2332, Sept. 2000.
- [8] F. J. Wentz, "Measurement of oceanic wind vector using satellite microwave radiometers," *IEEE Trans. Geosci. Remote Sensing*, vol. 30, pp. 960–972, Sept. 1992.
- [9] J. R. Piepmeier and A. J. Gasiewski, "High-resolution passive microwave polarimetric mapping of ocean surface wind vector fields," *IEEE Trans. Geosci. Remote Sensing*, vol. 39, pp. 606–622, Mar. 2001.
- [10] T. Meissner and F. Wentz, "An updated analysis of the ocean surface wind direction signal in passive microwave brightness temperatures," *IEEE Trans. Geosci. Remote Sensing*, vol. 40, pp. 1230–1240, June 2002.
- [11] F. Weng and N. C. Grody, "Retrieval of cloud liquid water using the Special Sensor Microwave Imager (SSM/I)," *J. Geophys. Res.*, vol. 99, no. D12, pp. 25 535–25 551, Dec. 20, 1994.
- [12] G. M. Skofronick Jackson and A. J. Gasiewski, "Nonlinear statistical retrievals of ice content and rain rate using passive microwave observations of a simulated convective storm," *IEEE Trans. Geosci. Remote Sensing*, vol. 33, pp. 957–970, July 1995.
- [13] J. D. Cunningham, F. L. Ricker, and C. S. Nelson, "The national polar-orbiting operational environmental satellite system future U.S. operational earth observation system," in *Proc. IGARSS*, Toulouse, France, July 21–25, 2003, pp. 351–356.
- [14] K. St. Germain and P. W. Gaiser, "Spaceborne polarimetric microwave radiometry and the Coriolis WindSat system," in *Proc. 2000 IEEE Aerospace Conf.*, Big Sky, MT, Mar. 18–25, 2000, pp. 159–164.
- [15] T. Kawanishi, T. Sezai, Y. Ito, K. Imaoka, T. Takeshima, Y. Ishido, A. Shibata, M. Miura, H. Inahata, and R. W. Spencer, "The Advanced Microwave Scanning Radiometer for the Earth Observing System (AMSR-E), NASA's contribution to the EOS for global energy and water cycle studies," *IEEE Trans. Geosci. Remote Sensing*, vol. 41, pp. 184–194, Feb. 2003.
- [16] J. Reisner, R. M. Rasmussen, and R. T. Bruintjes, "Explicit forecasting of supercooled liquid water in winter storms using the MM5 mesoscale model," *Q. J. R. Meteorol. Soc.*, vol. 124, pp. 1071–1107, 1998.
- [17] G. M. Skofronick-Jackson, A. J. Gasiewski, and J. R. Wang, "The influence of microphysical parameterizations on microwave brightness temperatures," *IEEE Trans. Geosci. Remote Sensing*, vol. 40, pp. 187–196, Jan. 2002.
- [18] J. N. Thepaut and P. Moll, "Variational inversion of simulated TOVS radiances using the adjoint technique," *Q. J. R. Meteorol. Soc.*, vol. 116, pp. 1425–1448, 1990.
- [19] P. Courtier, J.-N. Thepaut, and A. Hollingsworth, "A strategy for operational implementation of 4D-var using an incremental approach," *Q. J. R. Meteorol. Soc.*, vol. 120, pp. 1367–1387, 1994.

²Advanced Micro Devices (AMD) Athlon XP 2200 with 1 GB of RAM running Windows XP.

- [20] W. L. Smith, F. W. Harrison, D. E. Hinton, H. E. Revercomb, G. E. Bingham, R. Petersen, and J. C. Dodge, "GIFTS—The precursor geostationary satellite component of the future earth observing system," in *Proc. IGARSS*, Toronto, ON, Canada, June 24–28, 2002, pp. 357–361.
- [21] L. Phalippou, "Variational retrieval of humidity profile, wind speed, and cloud liquid-water path with the SSM/I: Potential for numerical weather prediction," *Q. J. R. Meteorol. Soc.*, vol. 122, no. 530, pp. 327–355, 1996.
- [22] P. Gabriel, J. Y. Harrington, G. L. Stephens, and T. L. Schneider, "Adjoint perturbation method applied to two-stream radiative transfer," *J. Quant. Spectrosc. Rad. Transf.*, vol. 59, no. 1/2, pp. 1–24, 1998.
- [23] E. Moreau, P. Bauer, and F. Chevallier, "Variational retrieval of rain profiles from spaceborne passive microwave radiance observations," *J. Geophys. Res.*, vol. 108, no. D16, p. 4521, Aug. 2003. DOI: 10.1029/2002JD003315.
- [24] A. J. Gasiewski and D. H. Staelin, "Numerical modeling of passive microwave O₂ observations over precipitation," *Radio Sci.*, vol. 25, no. 3, pp. 217–235, 1990.
- [25] A. J. Gasiewski, "Microwave radiative transfer in hydrometeors," in *Atmospheric Remote Sensing by Microwave Radiometry*, M. A. Janssen, Ed. New York: Wiley, 1993, ch. 3.
- [26] F. Weng and Q. Liu, "Satellite data assimilation in cloudy atmospheres: 1. Forward radiative transfer and Jacobian models," *J. Atmos. Sci.*, Sept. 2003.
- [27] E. A. Smith, P. Bauer, F. S. Marzano, C. D. Kummerow, D. McKague, A. Mugnai, and G. Panegrossi, "Intercomparison of microwave radiative transfer models for precipitating clouds," *IEEE Trans. Geosci. Remote Sensing*, vol. 40, pp. 541–549, Mar. 2002.
- [28] K. Stamnes, S.-C. Tsay, W. Wiscombe, and K. Jayaweera, "Numerically stable algorithm for discrete ordinate method radiative transfer in multiple scattering and emitting layered media," *Appl. Opt.*, vol. 27, pp. 2502–2529, 1988.
- [29] J. Lenoble, Ed., *Radiative Transfer in Scattering and Absorbing Atmospheres: Standard Computational Procedures*. Hampton, VA: Deepak, 1985.
- [30] L. Tsang, J. A. Kong, and R. T. Shin, *Theory of Microwave Remote Sensing*. New York: Wiley, 1985.
- [31] J. B. Sykes, "Approximate integration of the equation of transfer," *Mon. Not. R. Astron. Soc.*, vol. 11, p. 377, 1951.
- [32] M. Abramowitz and I. A. Stegun, *Handbook of Mathematical Functions*. New York: Dover, 1972.
- [33] T. Nakajima and M. Tanaka, "Matrix formulations for the transfer of solar radiation in a plane-parallel scattering atmosphere," *J. Quant. Spectrosc. Rad. Transf.*, vol. 35, pp. 13–21, 1986.
- [34] H. C. van de Hulst, *Multiple Light Scattering Tables, Formulas, and Applications*. New York: Academic, 1980, vol. 2.
- [35] M. Klein and A. J. Gasiewski, "Nadir sensitivity of passive millimeter and submillimeter wave channels to clear air temperature and water vapor variations," *J. Geophys. Res.*, no. D13, pp. 17 481–17 511, 2000.
- [36] L. D. Landau and E. M. Lifshitz, *Quantum Mechanics (Non-Relativistic Theory)*. London, U.K.: Pergamon, 1977, vol. 3.
- [37] A. J. Gasiewski, A. Voronovich, B. L. Weber, B. Stankov, M. Klein, R. J. Hill, and J. W. Bao, "Geosynchronous Microwave (GEM) sounder/imager observation system simulation," in *Proc. IGARSS*, Toulouse, France, July 21–25, 2003, pp. 1209–1211.



Alexander G. Voronovich was born in Moscow, Russia. He received the degree in physics and the Ph.D. degree in theoretical and mathematical physics, both from the Moscow Institute of Physics and Technology, Moscow, Russia, in 1972 and 1975, respectively, and the Doctor of Science degree in theoretical and mathematical physics from the Acoustical Institute, Moscow in 1988.

From 1975 to 1979, he was a Junior Research Scientist in the Acoustical Institute. In 1980, he joined P. P. Shirshov Institute of Oceanology as a Senior Research Scientist and in 1991 became a full Professor of physics at the Moscow Institute of Physics and Technology. From 1989 to 1993, he was a Head of the Laboratory of Acoustical Waves Propagation in the Ocean of the P. P. Shirshov Institute of Oceanology. He is currently an Oceanographer at the Environmental Technology Laboratory, National Oceanic and Atmospheric Administration, Boulder, CO. His research interests include wave scattering from rough surfaces, ocean acoustics, geophysical hydrodynamics, internal waves, linear and nonlinear theory of wave propagation, and radiative transfer theory.

Dr. Voronovich is a Fellow of the Acoustical Society of America and a member of URSI Commission F.



Albin J. Gasiewski (S'81–M'88–SM'95–F'02) received the M.S. and B.S. degrees in electrical engineering and the B.S. degree in mathematics, all from Case Western Reserve University, Cleveland, OH, in 1983, and the Ph.D. degree in electrical engineering and computer science from the Massachusetts Institute of Technology, Cambridge, in 1989.

From 1989 to 1997, he was Faculty Member within the School of Electrical and Computer Engineering, Georgia Institute of Technology (Georgia Tech), Atlanta. As an Associate Professor at Georgia Tech, he developed and taught courses on electromagnetics, remote sensing, instrumentation, and wave propagation theory. He is currently with the U.S. National Oceanic and Atmospheric Administration's (NOAA) Environmental Technology Laboratory (ETL) in Boulder, CO, where he is Acting Chief of the ETL Microwave Systems Development Division. His technical interests include passive and active remote sensing, radiative transfer theory, electromagnetics, antennas and microwave circuits, electronic instrumentation, meteorology, and oceanography.

Dr. Gasiewski is currently President of the IEEE Geoscience and Remote Sensing Society and was general chair of the 2nd Combined Optical-Microwave Earth and Atmosphere Sensing Symposium (CO-MEAS 1995). He organized the technical program for the 20th International Geoscience and Remote Sensing Symposium (IGARSS 2000) and is the named General Co-Chair of IGARSS 2006, to be held in Denver, CO. He is a member of Tau Beta Pi, Sigma Xi, the American Meteorological Society, the American Geophysical Union, and the International Union of Radio Scientists (URSI). He is currently serving as secretary of USNC/URSI Commission F. He has served on the U.S. National Research Councils Committee on Radio Frequencies (CORF) from 1989 to 1995.



Bob L. Weber received the B.S. and Ph.D. degrees in physics from The Ohio State University, Columbus, in 1965 and 1975, respectively.

Since 1974, he has been with the Environmental Technology Laboratory, National Oceanic and Atmospheric Administration, Boulder, CO. His research and interests have ranged from ocean remote sensing and electromagnetic scattering from rough surfaces, nonlinear wave theory, and turbulence, to remote sensing of the atmosphere using both active radars and passive radiometers. Currently, his work and interests focus on airborne and ground-based microwave radiometric observations of the atmosphere and surface and the assimilation of satellite microwave radiances into numerical weather prediction models.